École Polytechnique Fédérale de Lausanne
Laboratoire de Physique des Hautes Energies
Spring 2021

TP4b: The beta spectrometer

Author
Diego Mendoza

Supervisor
Dr. Maarten Van Dijk

Abstract

This study is focused on a Geant4 simulation [2] of a beta spectrometer [1], [8]. A improvement of the source generator is proposed and accepted against other generators through a Pearson's χ^2 test, under a significance level of 3σ for the specific case of the radionuclide ^{137}Cs. Other study of the energy resolution of the spectrometer with the implementation of a theoretical magnetic field [1] at different energies and solid angles of emission is done. The results are in bad agreement with experimental values obtained in [8] as the energy resolution starts to increase when a small solid angle emission is set. A solution for further studies is proposed to improve these results.

June 11, 2021

Contents

1 Introduction

The aim of experimental sciences is the building of knowledge through the measurement of natural phenomenons, where physical properties of matter and energy are involved. These properties are variables that commonly form continuous spectrum and whose values can vary with no step in a specific range. A spectrometer is a machine that can separate and measure these continuous variables using certain characteristics of the matter/energy involved in the phenomenon. For instance, magnetic spectrometers use a magnetic field to separate different types of matter depending on the value of their mass and charge through the Lorentz force. The shapes of the spectrometer and the magnetic field are designed in such a way that the particles deflected reach a detector when they have an specific energy value. These features are very useful to study radioactive nucleus where the particles emitted present a continuous distribution in energy as they can be selected varying the value of the applied magnetic field. This is the case of the beta spectrometer, used to study radioactive nucleus that decay through beta transitions.
The measurement of precise beta spectra is a current and relevant research topic for numerous fields. In nuclear reactors, precise knowledge of the energy of these beta spectra is needed, as most of nuclear waste generates heat through beta decay. Another example is the study of rare beta decays such as the neutrino-less double beta decay, where a precise measurement of beta spectra is fundamental for background rejection methods. Within the scope of the understanding of beta spectrum, beta spectrometers is a machine that plays an essential role. Its experimental use is commonly accompanied by simulations in order to assure the correct behaviour and setup of spectrometers. This enables to save time when measuring experimental data, taking into account that spectrometer experiments usually take days (even weeks) to complete.
This study is focused on a simulation in Geant4 [2], [4] of an existing beta spectrometer used to study many radionuclides, for example ^{137}Cs. The simulation was developed by F. Juget [1] and has been modified in two main aspects: the source generation in order to match theoretical beta-spectrum of ^{137}Cs and the implementation of an already proposed field parametrization in [1] to study the effect of source collimation. Firstly, Section 2 resumes the theoretical aspects in nuclear transitions and beta decay, also for the specific case of the ^{137}Cs radionuclide, with the main characteristics of the beta spectrometer. Secondly, the alternative source generators are presented in Section 3.1 and a Goodness-of-fit test is done in order to determine which one gives better results in comparison to a theoretical spectrum. Following, a discussion about the necessity of improving the magnetic map and extending the geometric limits of it is done in Section 3.2, together with a study on the energy resolution of the spectrometer simulation over the range [50,550] keV in energies using the proposed parametrized magnetic field. These results are finally discussed and concluded. An Appendix section includes all important considerations to understand the previous studies.

2 Theoretical aspects

2.1 Nuclear instabilities and beta transitions

The atomic nucleus is constituted by an integer number A nucleons, of which Z are protons, that give positive charge to it, and N = A-Z are neutrons. The mass of the nuclei is slightly lower than the sum of its constituents, as part of it is used as binding energy L and gives stability to the nuclei [18]:

$$m(Z,A)c^2 = Zm_pc^2 + Nm_nc^2 - L \tag{1}$$

where m_p is the proton mass, m_n is the neutron mass and $m(Z,A)$ is the mass of the nuclei with Z protons and N neutrons. The binding energy can be written as:

$$\mathrm{L} = a_\mathrm{v}\mathrm{A} - \mathrm{a_B A^{2/3}} - \mathrm{a_C Z^2/A^{1/3}} - \mathrm{a_a(A-2Z)^2/A} - \delta \tag{2}$$

being a_vA the volume energy and corrected by the terms: $a_sA^{2/3}$ as the surface energy, $a_a(A-2Z)^2/A$ the asymmetry energy, $a_cZ^2/A^{1/3}$ the coulomb repulsion and δ the Pairing term, which is equal to $a_pA^{-3/4}$ if N and A are even, $-a_pA^{-3/4}$ if N and Z are odd or zero if A is odd.

The beta transition occurs between isobars[1] as a proton is transformed into a neutron or vice-versa. There exists two types:

$$\begin{aligned} \beta^- : &\quad n \longrightarrow p^+ + e^- + \bar{\nu}_e \\ \beta^+ : &\quad p^+ \longrightarrow n + e^+ + \nu_e \end{aligned} \tag{3}$$

being e^- an electron, e^+ a positron, v_e an electron neutrino and $\bar{v}_e$ its antiparticle. Taking into account the nuclei involved in the reaction, the previous reactions can be written as:

$$\begin{aligned} \beta^- : &\quad {}^{\mathrm{A}}_{\mathrm{Z}}\mathrm{X} \rightarrow {}^{\mathrm{A}}_{\mathrm{Z+1}}\mathrm{Y}^{(*)} + \mathrm{e}^- + \bar{\nu}_\mathrm{e} \\ \beta^+ : &\quad {}^{\mathrm{A}}_{\mathrm{Z}}\mathrm{X} \rightarrow {}^{\mathrm{A}}_{\mathrm{Z-1}}\mathrm{Y}^{(*)} + \mathrm{e}^+ + \nu_\mathrm{e} \end{aligned} \tag{4}$$

The fact that the number A is constant in this transition enables us to impose the condition

$$\left.\frac{\partial \mathrm{M}}{\partial \mathrm{Z}}\right|_{\mathrm{Z=Z_A}} = 0 \tag{5}$$

giving the value of Z for the most stable isobar for the beta transition:

$$Z_A = \frac{A/2}{1 + \frac{a_cA^{2/3}}{4a_a}} < \frac{A}{2} \tag{6}$$

This means that the stable isobars have in general more neutrons than protons. The unstable isobars would decay until it reaches the stability through any of the two possible beta transition, depending on the excess of neutrons or protons. For those with $\mathrm{Z} > \mathrm{Z}_A$, they will decay through β^+ or electronic capture[2] and for those that $\mathrm{Z} < \mathrm{Z}_A$, through β^- until the stable isobar (Z_A,A) is

[1] Isobars are atoms with the same number A

[2] The electron capture is a similar reaction to the beta transition where an electron from a inner orbital reacts with a proton of the nuclei, giving as result a neutron and a neutrino: $p^+ + e^- \longrightarrow n + \nu_e$

reached. In the Figure 1 these differences can be seen, also when A is even and the Pairing term is introduced.

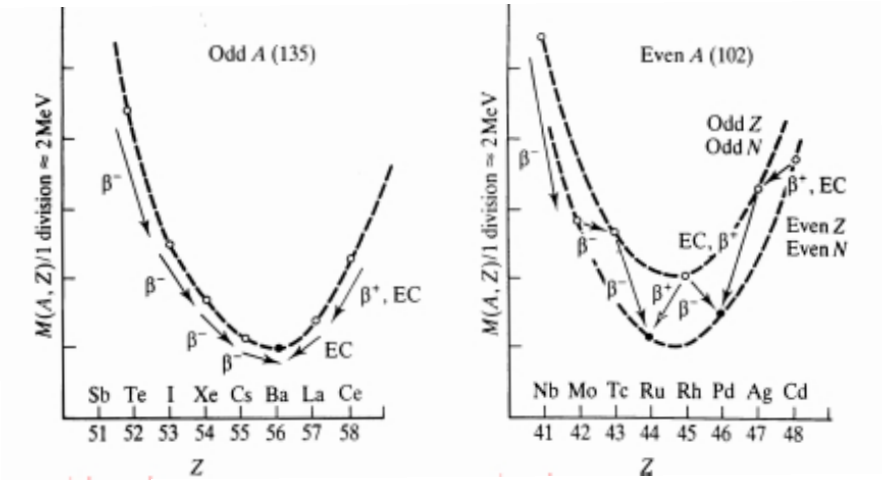

Figure 1: Left: A odd, one possible stable isobar. Right: A even, one or two possible stable isobars. Picture taken from [18]

The beta transition is a three-body decay. It means that the energy for each particle is not fixed and unpredictable, but the sum of the three energies is fixed and equal to the total energy of the radionuclide in the rest frame. Therefore, the spectrum expected for the electron would be continuous over the whole allowed range. From equation 4, the nucleus produced in the decay is in a excited state, so the emission of a gamma ray is followed. It can be possible that this photon interacts with one electron of an orbital in the atom and it is ejected, called internal (IC) conversion electron. In this case, it as a two-body reaction, so the energy of the electron is fixed and corresponds to the difference between the gamma energy and the energy level from where the electron has been emitted. The spectrum expected would be then a superposition of a continuous spectrum from the beta transition and and some discrete peaks called internal conversion peaks at very characteristic energy, depending on the emitted nucleus after the beta decay. An example of the expected spectrum is shown in [8].

2.2 The double focalizing magnetic spectrometer

The beta spectrometer is formed by a semicircular vacuum chamber, in which a pair of coils and pole pieces are located. The magnets have a geometry that generates a magnetic field which bends the electrons along a reference radius $r_0 = 18$ cm for which the electrons are deflected an angle 180°. The field gradient created is such that the electrons with a slight spatial and angular offset are focused in both vertical (X,Z) and horizontal (Z,Y) planes, towards the detector position. This is located at the point (+180,0,0) [mm] and has a circular shape of radius 4 mm, while the source is located at the point (-180,-320,0) [mm]. Near the source, it exits a collimator that allows for the

collimation in both vertical and horizontal planes, while near the detector there is other collimator that does in the horizontal plane. A more detail overview of the beta spectrometer employed for this study can be found in [8] and [1]. In Figure 2 a schema of the spectrometer is shown, taken from [15].

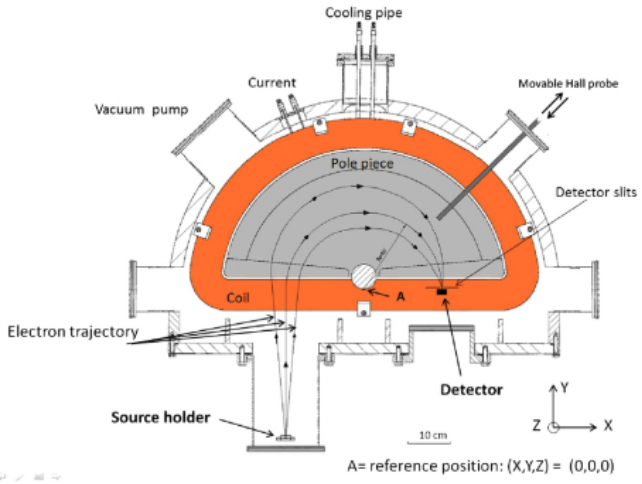

Figure 2: Diagram of the spectrometer from a top view

The magnetic field necessary to obtain a double focusing spectrometer is the following (in cylindrical coordinates) [1]:

$$\begin{aligned} B_Z &= B_0 \left[1 - \tfrac{1}{2}\left(\tfrac{r-r_0}{r_0}\right) + \tfrac{1}{4}\left(\tfrac{r-r_0}{r_0}\right)^2\right] \\ B_r &= ZB_0 \left[\tfrac{1}{2r_0} + \tfrac{r-r_0}{2r_0^2}\right] \\ B_\phi &= 0 \text{ by symmetry} \end{aligned} \tag{7}$$

where $r = \sqrt{x^2 + y^2}$ and B_0 the nominal magnetic field for the reference radius r_0 and Z=0. The relation between the magnetic field and the momentum of an electron traveling at the reference trajectory is given by:

$$p[\text{MeV}/c] = 0.3B_0[mT]r_0[m] \tag{8}$$

or in terms of the kinetic energy of the electron:

$$T[\text{MeV}] = \sqrt{(0.3Br_0)^2 + m_e^2} - m_e \tag{9}$$

where m_e is the mass of the electron. Using the equations 8 or 9, the magnetic field is set to select the particles with the momentum/energy desired to hit the detector through the reference trajectory. The opening of the source collimator will also determine a proper selection of the energy of the electrons.

2.3 β^- transitions of ^{137}Cs

Cs-137 is a radionuclide that decays by beta minus emission to the ground state of ^{137}Ba (5.6 %) and the 661 keV isomeric level of ^{137}Ba (94.4 %). It has half-life $T_{1/2} = 30.05$ years and energy realise $Q = 1175.63$ keV. It presents three possible β^- transitions [12]:

- First unique-forbidden. This transition is characterized by a difference in the total angular momentum between the daughter and the mother nuclei of $\Delta I = \pm 2$ units and a change in parity $\Delta\pi = 1$ [13]. With a maximum energy of 513.97 (17) keV, this transition is the most probable, 96.36 (28) % .
- Second unique-forbidden. Transition in which the parity between the daughter and the mother nuclei is conserved but there is a difference $\Delta I = \pm 3$ units [6]. This transition is a specific type of the 2nd Forbidden. The maximum energy is 892.1 (2) and it is the less probable, 0.00061 (8) %.
- Second-forbidden. The parity between the daughter and the mother nuclei is conserved but there is a difference $\Delta I = \pm 2, \pm 3$ units [6]. The maximum energy is 1175.63 (17) keV and the probability of transition 5.64 (28) %

3 Results of the simulations

3.1 Source generation

The discrepancies found in [16] between experimental measurements through the beta spectrometer and the Geant4 simulation claim that some parts of it need to be improved in order to match experimental data. The source generator seems as a good candidate as the original simulation makes use of a purpose-made beta decay generator for some radionuclides. A comparison to a theoretical spectrum has been done. The program Betashape [9], [10], provided by the Laboratoire National Henri Becquerel, calculates the probabilities and uncertainties of a transition for the kinetic energy range of a beta decay using the nuclear data available in [12]. For the case of Cs-137, this range is from 0 to 1175.63 keV. Following the discussion in appendix B, a total number of 10^8 events has been simulated for the source generator. The histogram obtained from the Betashape program was normalized and has been scaled to the same number of events. This result[3] is shown in the Figure 3. The main difference between the original generator spectrum and the theoretical one is at high energies. From the logarithmic scale image, the critical point is located near 500 keV, from where the spectra starts behaving differently. This point corresponds to 513.97 keV and is the limit for the first beta transition, the first unique-forbidden and the most probable one in the beta decay of Cs-137, see Section 2.3. For energies higher than this limit, the two remaining beta decays (second unique-forbidden and second-forbidden) differ notably, so one can conclude that the main part where to improve the source generator should be up to this limit.
The proposed source generator to improve the ^{137}Cs spectra is G4RadioactiveDecay, provided by Geant4 for radioactive decays [11]. Again, a total number of 10^8 events has been simulated. The result is shown in Figure 3.

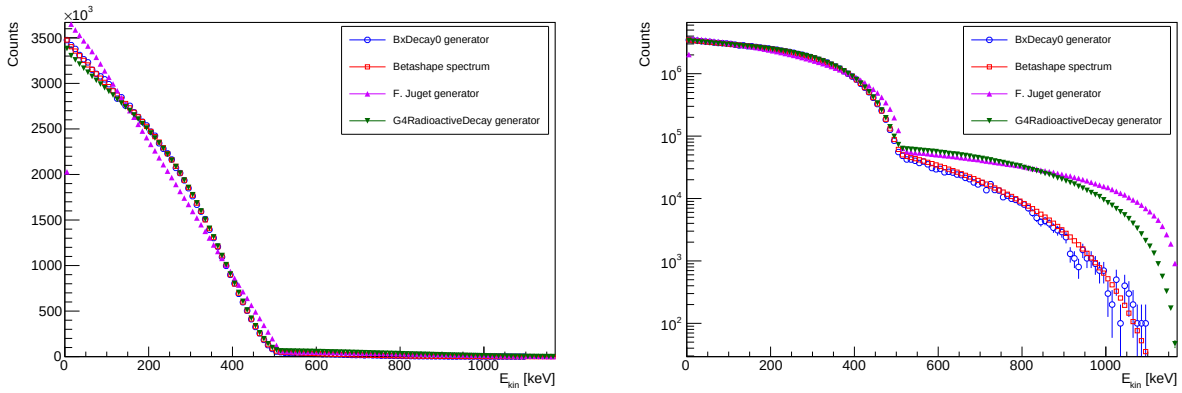

Figure 3: Plot of the four beta spectrum (left), in log scale (right)

In order to do a strict comparison of the generators described before with the theoretical spectrum, a Pearson's Chi-square Test has been done for each case, with 116 as degree of freedom (ndf)[4]. One of the results of the test are the residuals, explained in Appendix C. They are shown in Figure

[3] To do the comparison all IC peaks have been removed as the main reason of the discrepancy between the spectra were due to the beta transition

[4] The degree of freedom for the comparison between histograms corresponds to the the total number of bins -1, according to [19]

(4) for the two source generators. In the image (5), the QQ plots of the residuals, explained in Appendix C, using a normal distribution are also shown for these two source generators.

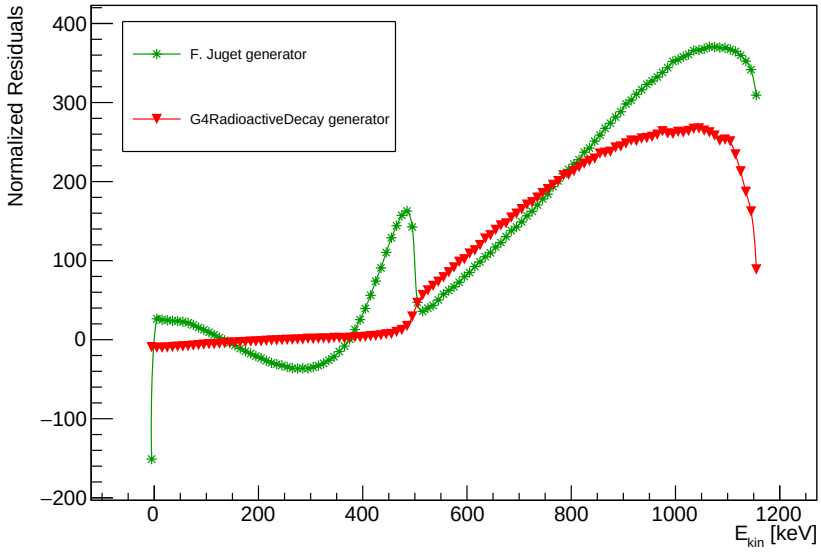

Figure 4: Plot of the normalized residuals for two generators

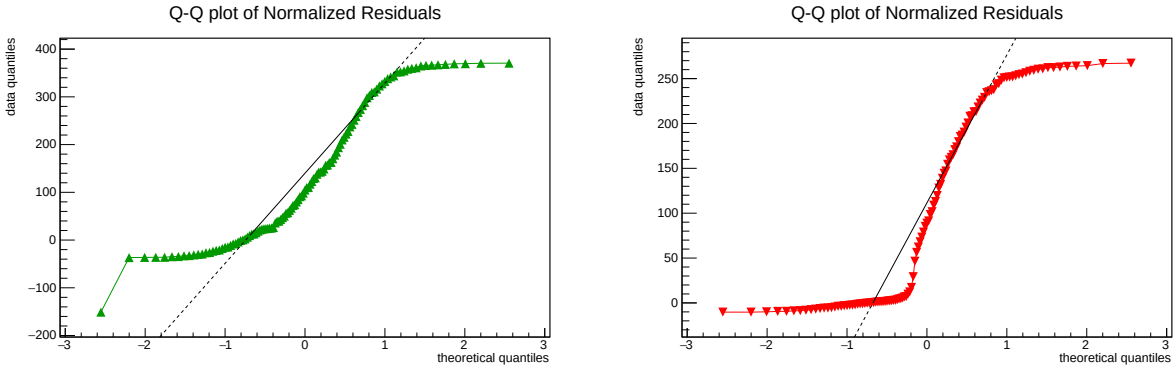

Figure 5: Plot of the QQ plots of the residuals for the original (left) and G4RadioactiveDecay (right) generators.

After replacement of the original generator by the G4RadioactiveDecay generator of Geant4, it was found that it represents a substantial improvement. From Figure 4, the residuals from the G4RadioactiveDecay generator are close to zero for half of the full range of energy, what shows that it improves the results with respect to the original generator. Nevertheless, they become larger at high energies. This new generator fails to improve the results at high energies, which was the main part of the spectra to focus. The reason is that it generates the unique second-forbidden transition and the second-forbidden in the same way as an unique first-forbidden transition, neglecting angular corrections due to larger differences in the total angular momentum between the mother and the daughter nuclei, as explained in Section 2.3.

To solve this issue, the BxDecay0 C++ library [17] has been used to generate the beta spectrum for Cs-137. This library provides a powerful tool to generate nuclear transitions where double beta decay processes are involved, as well as for standard radioactive isotopes. It also has into account angular corrections for different β^- transitions, what would mean that the spectra at high energies could improve respect to the previous source generators. The results are shown in Figure 3 for the generation of 10^8 events and in Figure 6 for the residuals and QQ plot of the residuals.

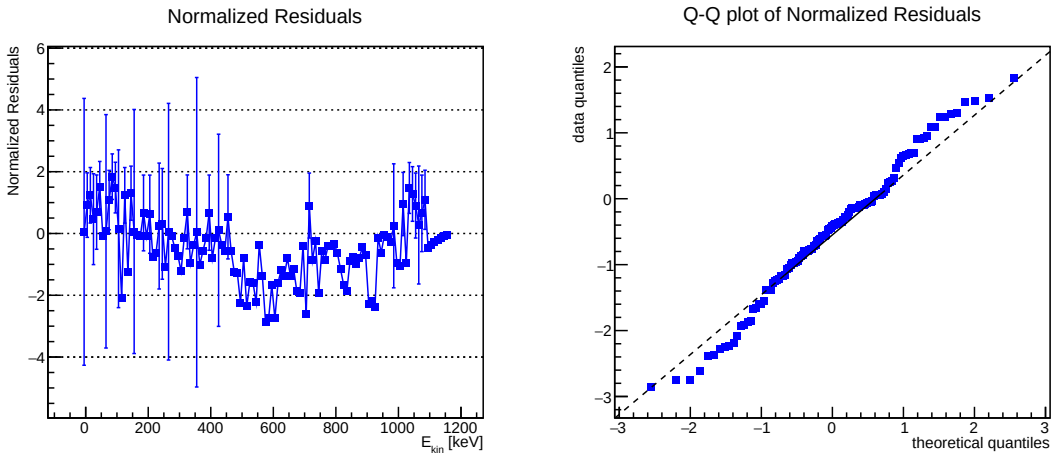

Figure 6: Plot of the normalized residuals and QQ plots of the normalized residuals for BxDecay0 generator

The maximum of the residuals are around two order of magnitude lower than the maximum values for the previous generators, and the QQ plot of the residuals is not deviated from the theoretical line at high energies, showing a better concordance to the theoretical spectrum.
Following the concepts and reasoning in Appendix C, a significance level of 3σ was chosen for the previous tests, which corresponds to a P-value of 0.00135. Therefore, any hypothesis for which the test gives a P-value greater than this one will be accepted. The results of the Chi-square test are presented in the table 1.

Source generator	χ^2	$\frac{\chi^2}{ndf}$	P-value
F. Juget generator	29900000	258000	0[5]
G4RadioactiveDecay	4110000	35400	8.3×10^{-17}
BxDecay0	152.74	1.32	0.0126

Table 1: Results of the Chi-square test for the proposed hypothesis.

A value of $\frac{\chi^2}{ndf}$ close to one means a good result of the test for that case. Therefore, the BxDecay0 generator is in reasonable agreement with the Betashape data as the normalized Chi-square is close to unity and it gives a P-value greater than the significance level chosen, so this generator is accepted as hypothesis. The rest of the generators are rejected as the P-values are very small and also the normalized Chi-square values are far from unity. The previous graphics help to understand

[5]The reason why this result is zero is due to the program used to run this test (ROOT) makes this approximation. Other numeric calculus has been done, showing that this number is 4×10^{-72070}

these results. Concluding this part of the study, the BxDecay0 library is accepted as the new source generator for the beta spectrometer simulation, already available and implemented on the program by the author.

3.2 Study of the energy resolution and magnetic efficiency

A previous study of the energy resolution in the simulation [16] shows a large disagreement respect to the experimental data at $IC_{2,0K}$ peak of ^{137}Cs at 624.218 keV. The reason proposed for this difference is the following: the magnetic field map, shown in Figure 7, was generated by F. Juget through the program POISCR in [1]. It simulates the real magnetic field produced by the magnets. This map presents an important limitation in the Y direction inside the magnetic chamber of the spectrometer, as it is schematically represented in Figure 8. For values of $|y| > 4$ cm, the magnetic field is not available so it is taken as zero in the simulation. This makes that the some particles emitted with a large opening angle would leave the magnetic chamber at some point, affecting the energy resolution and efficiency measurements and therefore they do not match to experimental data.

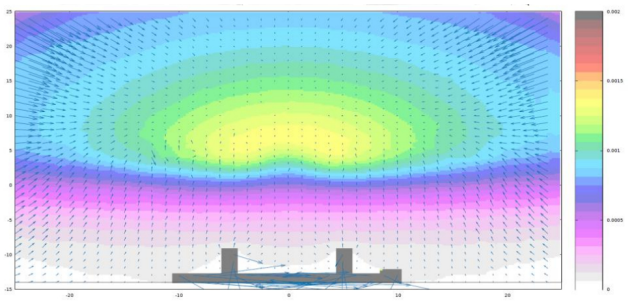

Figure 7: Representation of the magnetic field map for the beta spectrometer in the plane Z=0 done in [1] and visualized using FLUKA [7], [3]

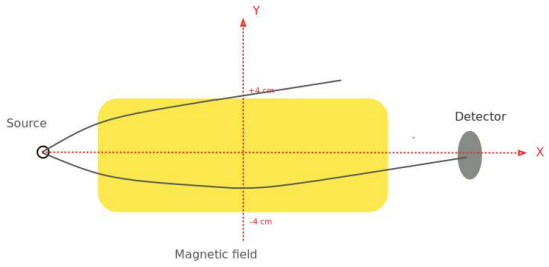

Figure 8: Simple schema of the magnetic field limitation.

A good solution to this problem is to extend the simulated magnetic field to the full interior of the magnets. In order to do this, it is necessary to implement the design of the magnet in the B-field simulation program and recalculate the magnetic map, extending the limits commented before. Nevertheless, this task could not be done due to a lack of time after completing the study of the source generator, as it is necessary to get familiar with this new program to simulate the magnetic field. Instead, the implementation of the theoretical magnetic field, equation 7, can be interesting in the study of the energy resolution of the detector. Even though the suggested solution does not represent a very realistic model for the B-field, the limits of the original magnetic map can be extended to the entire geometry of the detector. As this fact has been assumed to be the principal cause of the discrepancy between measurements and simulation results, the new study extending the limits help to understand how much the simulation can be improved if the magnetic map is extended and recalculated in the future.
To study the energy resolution under this magnetic field, the source generator has been changed to produce only mono-energetic electrons in the solid angle desired. Doing the analysis over the full

spectrum is a long process from the computational view, so the initial energies have been varied from 50 to 550 keV, in steps of 50 keV. For each energy, the value of the magnetic field at the reference trajectory, B_0, is modified using the equation 9. It is relevant to choose an appropriate step size and range to do this scan, such that the data obtained is enough to do a fit and estimate the resolution. From [16], it was expected that a Gaussian fit would be suitable for most if not all of these situations. Therefore, using the concepts presented in Appendix D, the energy resolution is proportional to the standard deviation obtained from a fit, so in further results only the standard deviation will be presented. The smaller that the standard deviation is, the lower the energy resolution is, what means the better to difference peaks with close central values. From the analysis in the full range done in [16], the standard deviations obtained approximately correspond to 1% of the kinetic energy of the particles generated, E_0. This result is also validated in preliminary simulations before doing a wide scan. Then, proposing a scan varying the magnetic field in the range $[E_0 - 4\sigma, E_0 + 4\sigma]$ and assuming that obtaining at least 4 points per σ is a good compromise for a posterior fitting, the total number of steps to do is 32. Therefore, the step can be estimated using:

$$\delta_{T_{B-field}} = \frac{8\sigma}{32} = \frac{80.01E_0}{32} = \frac{0.01E_0}{4} \tag{10}$$

The step would be smaller for low E_0 and it increases when E_0 does. For all E_0, the solid angle of emission is also scanned, which simulates varying the slit opening at the source collimator, as it is explained in Appendix A. In steps of 0.015625 rad, the angle ϕ_1 is scanned from 0.25 to 0 and ϕ_2 from 0.125 to 0. This corresponds to reduce the length opening 1 cm per step, 0.5 cm in each edge, for both the vertical and the horizontal slits until a line emission is reached. A total number of 153 different solid angles of emission are simulated for each E_0.
In Appendix E, all the data obtained for the mentioned simulations is shown. The case of $E_0 = 500$ keV is shown in Figure 9.

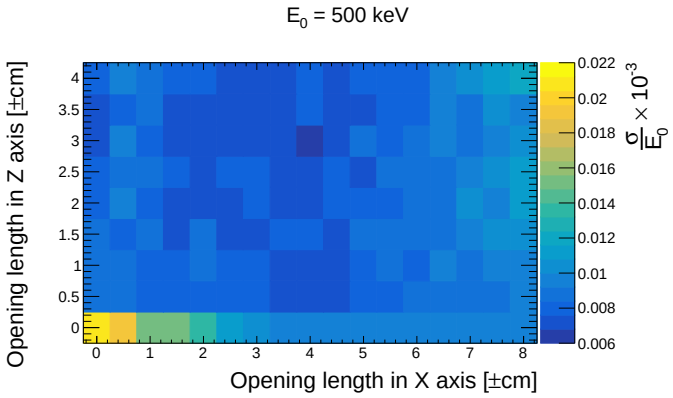

Figure 9: Histogram representing $\frac{\sigma}{E_0} \times 10^{-3}$ in terms of the horizontal and vertical slit opening for primary energy 500 keV

From the figures mentioned, the first result observed is the dependence of the energy resolution in the primary kinetic energy E_0. This is a reasonable result as for low E_0, the values of the magnetic field at the reference trajectory, B_0, that are scanned are also small values. Then, the particles need more steps in the magnetic field scan to form the Gaussian distribution that has been mentioned before. The graphics in Figure 10 how the standard deviation increases when E_0 is increased.

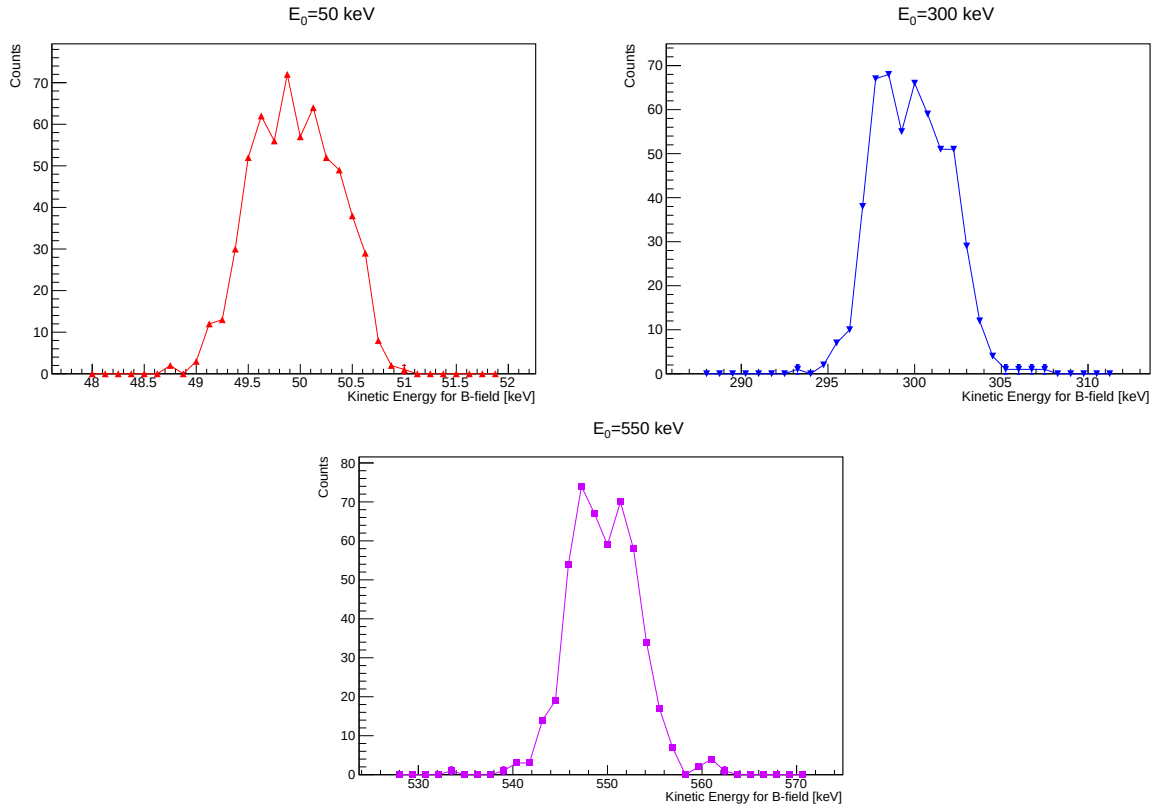

Figure 10: Energy resolution for ±4 cm of slit opening in both horizontal and vertical slits

From all E_0, it is clear that σ increases when the slits are opened to their maximum value. It deceases when the opening is reduced for the horizontal or vertical slit, being much more noticeable when both are reduced so we get to the central bins of the histograms. From [8], the values of FWHM obtained for an opening of 1 mm in the detector slits are 4.46 keV at 624.218 for the IC K line of ^{137}Ba and 3.08 keV at 240.41 keV and 3.23 keV at 266.86 keV for the IC K lines of ^{133}Cs keV. These values correspond to $\frac{\sigma}{E_0}$ equal to 3.04×10^{-3}, 3.94×10^{-3} and 5.15×10^{-3} respectively. From the measurements obtained and represented in the histograms in Figures 14 and 15, all values are larger than these three. However, the most surprising result is that the energy resolution starts when the opening is smaller that the value ±1 cm for both slits. The energy resolution is expected to decrease until the line emission is reached, being this configuration the most favourable one. It was supposed that the previous experimental values could be reached reducing the solid angle emission. Simulated data disagrees with this assumption. A new scan has been done at small opening angles and with reducing the step size. From 0.015625 rad for both ϕ_1 and ϕ_2 and in steps of 0.003125 rad until reach to 0 rad. This corresponds to reduce the length opening 2 mm per step, 1 mm in each edge, for both the vertical and the horizontal slits until a line emission is reached. A total number of 36 different solid angles of emission are simulated for each E_0 again. This data is available in Figures 16 and 17, in Appendix E. Figure 11 shows these results for the specific case of $E_0 = 500$ keV.

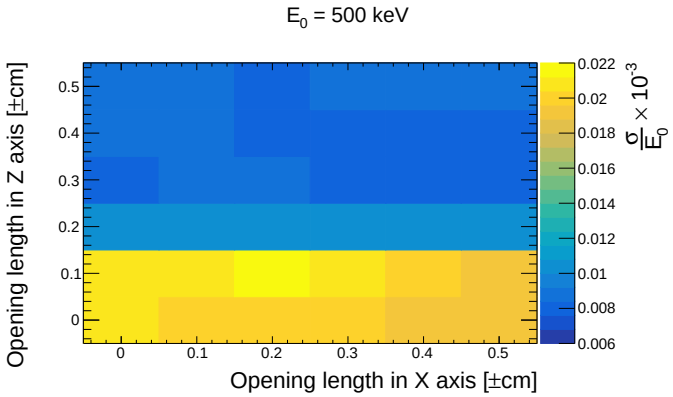

Figure 11: Histogram representing $\frac{\sigma}{E_0} \times 10^{-3}$ in terms of the horizontal and vertical slit opening for primary energy 500 keV with small step size of the slit opening

In this case, the increase of the energy resolution for small opening slit size is much more noticeable, specially for the horizontal slit. The reason for this is that, with this new magnetic map, once that the electron beam is hitting the detector, it needs a large number of steps in the magnetic field scan to stop reaching it when the slit opening is very small for the horizontal or vertical slits. This means that the energy resolution cannot be improved more when the solid angle of emission is reduced. To complete this reasoning, the different distributions in the energy resolution for $E_0 = 500$ keV are shown for different openings in Figure 12 for the first data simulated with big step size in the solid angle of emission and Figure 13.

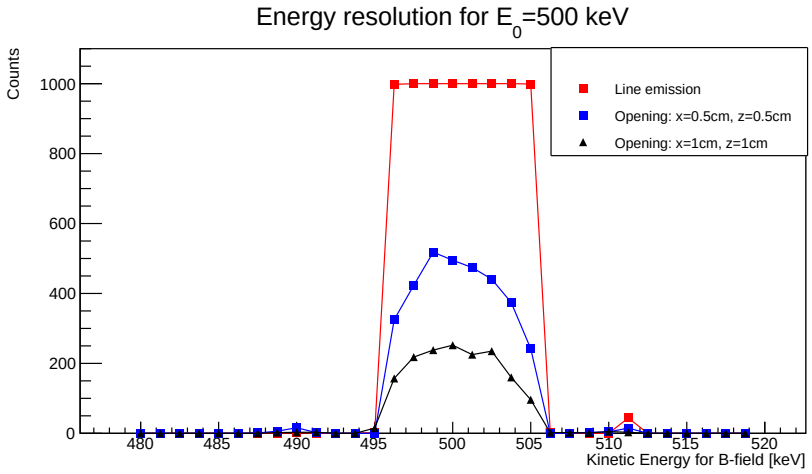

Figure 12: Energy resolution for different slit opening at $E_0 = 500$ keV

The conclusion of this part of the study is that the energy resolution cannot be reduced more than a certain value for this magnetic map as for very small solid angle emission it corresponds to the size of the detector. This also explains that the energy resolution starts increasing when small solid angle of emission is reached, as the distribution changes from Gaussian to a rectangular function. A solution proposed to improve this result would be use another collimator at the detector position. In this way, the width of the distributions shown in Figures 12 and 13 could decrease, depending on the features of this new collimator and it size. The Gaussian distribution could be used for small solid angle emission, so this effect would not appear until a certain point, which is inevitable.

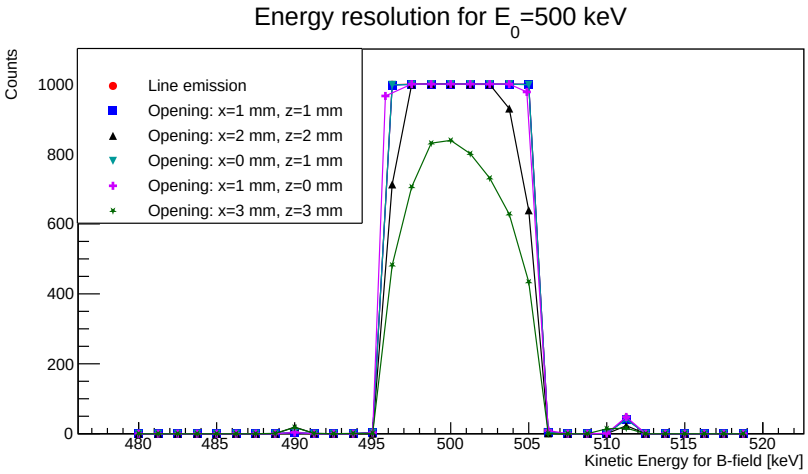

Figure 13: Energy resolution for different slit opening at $E_0 = 500$ keV and small step size for slits

In reality, the efficiency of the spectrometer would be too small that maybe this configuration is impractical. However, the fact that the angle of emission can be chosen in the simulation helps to neglect this effect.

4 Conclusion

The improvement of the source generator was one of the solutions proposed to solve the discrepancies found between measurements and simulated data. The first generation of events by the original generator shows that both spectrum have different form, specially at high energies of emission. The first suggested generator, G4RadiactiveDecay, is able to slightly improve the data but it fails to approach to the theoretical spectra in the range of high energies. The second generator, BxDecay0, makes a relevant improvement in this range, as well as at the rest of energies. A Pearson χ^2 test has been done to test these generators. The BxDecay0 is accepted under a level of significance of 3σ, giving a P-value of 0.0126. The rest of generators fail the test so they are rejected as hypothesis. The new generator is implemented in the beta spectrometer simulation and available for it use in future measurements. The study of the energy resolution is done with the implementation of the magnetic field proposed in [1]. The main advantage is that the geometric limitation in the Y direction is now solved as this magnetic map is extended over all the chamber of the spectrometer. Simulations show that the energy resolution of the spectrometer cannot be reduced more than a certain value. When the solid angle of emission becomes very small, the distribution of the peak changes from a Gaussian to a rectangular function, what makes that the values measured for the energy resolution start to increase. This issue is due to the magnetic map used and the geometry of the detector. A proposed solution for future studies in order to solve this issue is to implement a collimator at the detector position in the simulation of the spectrometer. Depending on the size chosen for this collimator, the energy resolution could be reduced until a desired value. The effect of the efficiency is not important in the simulation as the direction of emission can be set. However, it would be very significant for the intensity of the signal in real measurements.

Appendices

A Angular correlation in γ and IC electrons after the β decay

The probability of the direction of emission for the electron in the beta decay[4] is uniformly distributed in the unit sphere under the presence of no magnetic field. In the present case, the geometry of the magnets in the beta spectrometer creates a negligible magnetic field at the source position, so the previous assumption can be done. In the original implementation of the simulation, electrons from the beta decay were only uniformly emitted in a direction that had a chance to reach the detector [1]. This direction was determined by the angles, at the source point, α_1 and α_2 that give the total opening width in the X-axis and Z-axis, respectively (see Figure 2). This is a way to simulate the behaviour of the source collimator located at (-180,0,0) [mm] in the beta spectrometer. Limited by the physical dimension of the spectrometer and the magnetic field map, the optimal angles to emit particles that would reach the detector were determined in [1] to be $\phi_1 = \pm 0.25$ and $\phi_1 = \pm 0.125$ rad. This gives a shape of a four-sided right rectangular pyramid, corresponding to a total area at the source collimator $A = 128$ cm^2 with rectangular shape and a solid angle $\Sigma = 0.125$ rad [14], which is near 1% of the unit sphere (4π). Adapting the simulation to generate particles in a specific solid angle of emission would then mean saving a large amount of computational time.
If an uniformly probable emission of the electron in the solid angle chosen is assumed, this would affect the direction of emission of the rest of the particles, and specially for our interest, the internal conversion electrons from the ^{137}Ba. However, the electrons reaching the detector after travelling through the spectrometer are measured as counts, which means that it is impossible to distinguish between those emitted in a beta transition and the IC electrons from the ^{137}Ba. Moreover, the radioactive source is in reality not deposited in vacuum as in the simulation, but as a liquid instead [8], [15], which evaporates and leaves behind a salt. This means that the ^{137}Ba nucleus are practically fixed after that the beta decay occurs, which converges to an isotropic emission for the gammas rays and IC electrons from the ^{137}Ba. Therefore, electrons from the beta decay and the ^{137}Ba decay can be considered independently and not as part of the same event.
In the modified simulation, a new source generator has been developed in order to emit all particles that participate in the β decay of ^{137}Cs and in the subsequent decay of ^{137}Ba in a specific solid angle as fixing the direction of emission for both primary electrons from the beta decay and IC electrons is a good approximation that enables saving a lot of computational time for the simulation.

B Estimating the statistical error for the simulated data

In section 3.1, it is important that the histograms have similar statistical errors to do a proper comparison. The total number of events can be chosen by requiring that the statistical error on the resulting histogram is comparable to the error in the Betashape data [9], [10]. The data given by the Betashape program is a weighted histogram, while the histogram obtained from the Geant4 program will be unweighted, so the bin error is propagated as:

$$\delta_i = \frac{\sqrt{n_i}}{n_i} \tag{11}$$

[4] Reasoning valid also for the neutrino or the Ba-137 nuclei

where n_i is the number of events in the bin i. If we set this error to be of the same order of the normalized bin error for the theoretical histogram, $\frac{\delta_{i_t}}{n_{i_t}}$, where δ_{i_t} is the error and n_{i_t} the bin content of the bin i, the number of events in the bin to have good statistics, n_i, can be estimated. Finally, using that the theoretical histogram is normalized, each bin content corresponds to the probability n_{i_t} of generating an event and obtaining an energy falling in this bin. Then, the total number of events to simulate can be estimated as follow:

$$N_{tot} \approx \frac{n_{i_t}}{\delta_{i_t}^2} \tag{12}$$

With this calculus, one can guess that the statistical error of the bin that is considering would be comparable to the error in the reference bin of the theoretical histogram to compare with. Ideally, if this calculus is done for the smallest bin error in the theoretical data, the total number of events to simulate that gives better statistical error is estimated. However, this value could correspond to a very large number, impossible to generate in practice. For the present case, the theoretical data from the Betashape program gives 3×10^{-13} as the smallest error, for a bin content of 1.056×10^{-10} at 1168 keV. This number would require a total number of 1.5×10^{15}, what is impossible to generate in reality. Therefore, it is not possible to generate a histogram in which all the bin have a comparable error with the Betashape data, specially for high energies, where the bin content is very small. A good compromise would be to obtain as many bins with a comparable error to the theoretical data and a reasonable number of events to generate. For example, at 620 keV the values are 1.12×10^{-6} as error, and 1.301×10^{-4} and bin content. This number would require a total number of 1.03×10^{08} events to generate, what is now a reasonable number to simulate. The values of energy lower than this limit have an error higher[5], so half of the range of the histogram is assured to have a compatible error with theoretical data.

C Pearson's Chi-square Test for Histograms

In the concern of testing a null hypothesis H_0[6] with a test statistic T at a significance level α and in a critical region ω_α, goodness-of-fit tests compare experimental data with their probability density function under H_0, giving as result a quantity called P-value. This is interpreted as the probability of repeating the measurements many times and obtaining the data at least as far away from H_0 as the observed data. Therefore, its size specifies the agreement between data and the hypothesis. The acceptance/rejection of the hypothesis depends on the significance level Z chosen, which is other way of expressing the P-value. In High Energy Physics, a significance level of 5σ (Z=5) usually claims a discovery and 3σ (Z=3) is used for an evidence when testing against the null hypothesis. The relation between the significance level and the P-value can be written as:

$$p = \frac{1 - \mathrm{erf}(Z/\sqrt{2})}{2} \tag{13}$$

where $erf(z) = \frac{2}{\sqrt{\pi}} \int_0^z e^{-t^2} dt$ is the error function. For a certain significance level, if the statistic

[5] From what we can observe in the Cs-137 spectra, the number of counts decreases when the kinetic energy is higher. This justifies that the bins before this limit will be compatible with the Betashape data in terms of error

[6] In the present case, the null hypothesis is that the two histograms to compare through represent the same distribution so they are similar

test gives a P-value lower, the hypothesis is then rejected. Otherwise, it is accepted under the significance level chosen.
In data analysis, the comparison of histograms is commonly done by the χ^2 test of homogeneity. This test depends on the characteristics of the histograms, mainly if they are weighted or unweighted. The paper [5] explains the techniques to use for each case. The theory will be summarized for the comparison of unweighted-weighted histograms.
The number of events in the i'th bin for the unweighted histogram is n_i, a random variable approximately distributed by the Poisson distribution $e^{-Np_i}\left(Np_i\right)^{n_i}/n_i!$, and for the weighted histogram w_i approximately distributed by a normal distribution $N\left(Wp_i, \sigma_i^2\right)$. Here, σ_i^2 is the variance of the weights w_i and N and W are the total number of events of each histogram, $N = \sum_{i=1}^{r} n_i$ and $W = \sum_{i=1}^{r} w_i$. Formulating the hypothesis of identity: "There exist r constants p_1,...,p_r with $1 = \sum_{i=1}^{r} p_i$ such that p_i is the probability of a measured value to belong to the ith bin for the unweighted histogram and Wp_i for the weighted histogram", the maximum likelihood estimator of p_i is:

$$\hat{p}_i = \frac{Ww_i - Ns_i^2 + \sqrt{\left(Ww_i - Ns_i^2\right)^2 + 4W^2 s_i^2 n_i}}{2W^2} \tag{14}$$

where s_i^2 is the sum of squares of weights in the ith bin.
Therefore, the chi-square test is formulated as:

$$\chi^2 = \sum_{i=1}^{r} \frac{\left(n_i - N\hat{p}_i\right)^2}{N\hat{p}_i} + \sum_{i=1}^{r} \frac{\left(w_i - W\hat{p}_i\right)^2}{s_i^2} \tag{15}$$

The difference between w_i and the $W\hat{p}_i$ is defined as the variance z_i^2:

$$\begin{aligned} z_i^2 = N\hat{p}_i\left(1 - N\hat{p}_i\right)\left(\frac{Ws_i^2}{\sqrt{\left(Ns_i^2 - w_i W\right)^2 + 4W^2 s_1^2 n_i}}\right)^2 \\ + \frac{s_i^2}{4}\left(1 + \frac{Ns_i^2 - w_i W}{\sqrt{\left(Ns_i^2 - w_1 W\right)^2 + 4W^2 s_i^2 n_i}}\right)^2 \end{aligned} \tag{16}$$

and the residuals:

$$r_i = \frac{w_i - W\hat{p}_i}{z_i} \tag{17}$$

This residuals are random variables that follow a normal distribution of mean $\mu = 0$. If the residuals are normalized, then the standard deviation of their distribution is equal to one. A useful diagnostic to analyse the result of the test is to inspect the residual plot, where each residual is represented versus the bin center where it has been obtained. One should not find any trend in the plot, as a tendency for negative residuals at small values and positive residuals for large values of bin centers. Also, one should also observe a constant spread of the residuals.
Other way of analyzing the test is studying the Q-Q plot (data quantiles versus distribution quantiles). This is a graph of the order statistics from the residuals, r_i, versus the expected order statistics of the standard normal distribution, z_i. The residuals are ordered from smallest values to largest, being now each r_i. To calculate the expected order statistics, also known as rankits, an

useful approximation is

$$z_i = \Phi^{-1}\left(\frac{i-a}{n+1-2a}\right) \tag{18}$$

where Φ is the standard normal quantile function, n is the sample size and $a = \frac{3}{8}$ if $n < 10$ or $a = 0.5$ if $n > 10$ [19]. If one plots the order statistics versus the rankits, a straight line through 0 and with slope 1 would be expected under the assumption that measurements and theoretical data follow the same distribution.

D Energy resolution

The energy resolution of a detector is the capability of distinguish between radiation with different energy. In the case of a counter detector, it cannot measure the energy of the incoming radiation. Therefore, it is important to adjust the energy resolution to the best value in order to do precise measurements. To measure the energy resolution for a slit size, IC peaks are used as they are delta distributions. Then, selecting different energies through the magnetic field around the IC peak, the number of particles detected has a Gaussian distribution. Measuring the standard deviation of the Gaussian, σ, one can obtain the full width at half maximum (FWHM) and therefore the energy resolution of a spectrometer.

$$R = \frac{\text{FWHM}}{\mu} = \frac{2.35\sigma}{\mu} \tag{19}$$

E Histograms obtained for the energy resolution analysis

This Appendix includes the histograms filled with the data obtained in the simulations explained in Section 3.2. For the case of big step in the slit opening (1cm), the data is shown in Figures 14 and 15

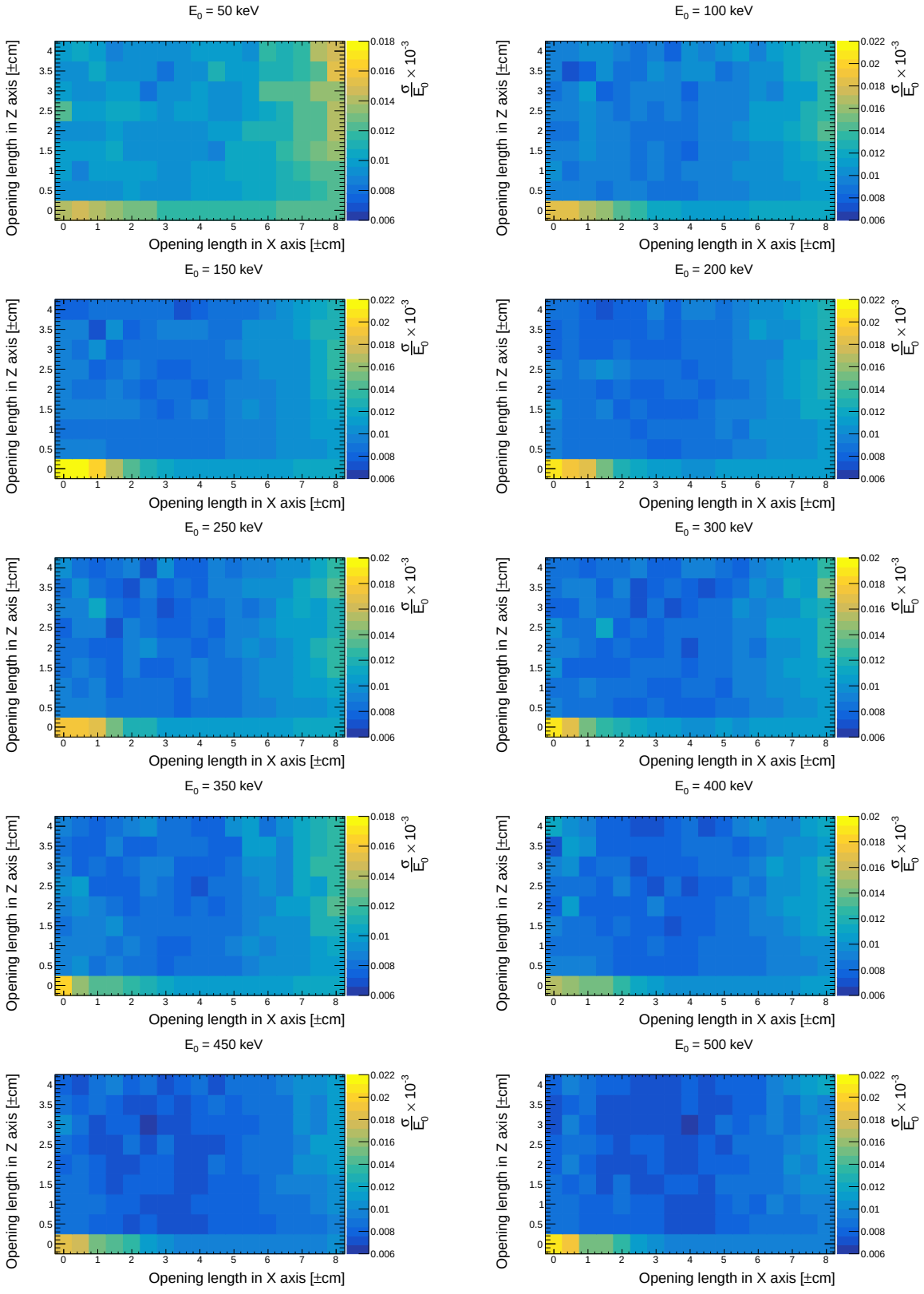

Figure 14: Histograms representing $\frac{\sigma}{E_0} \times 10^{-3}$ in terms of the horizontal and vertical slit opening for primary energies from 50 to 500 keV

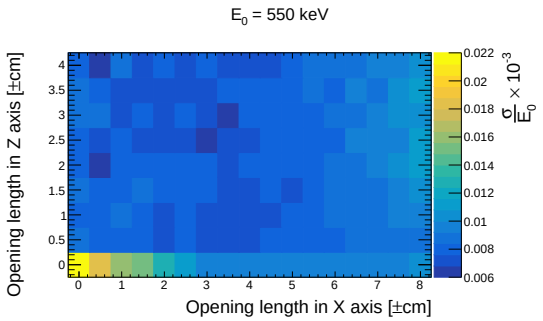

Figure 15: Histogram representing $\frac{\sigma}{E_0} \times 10^{-3}$ in terms of the horizontal and vertical slit opening for primary energy 550 keV

For the case of small step in the slit opening (0.2 cm), the data is shown in Figures 16 and 17.

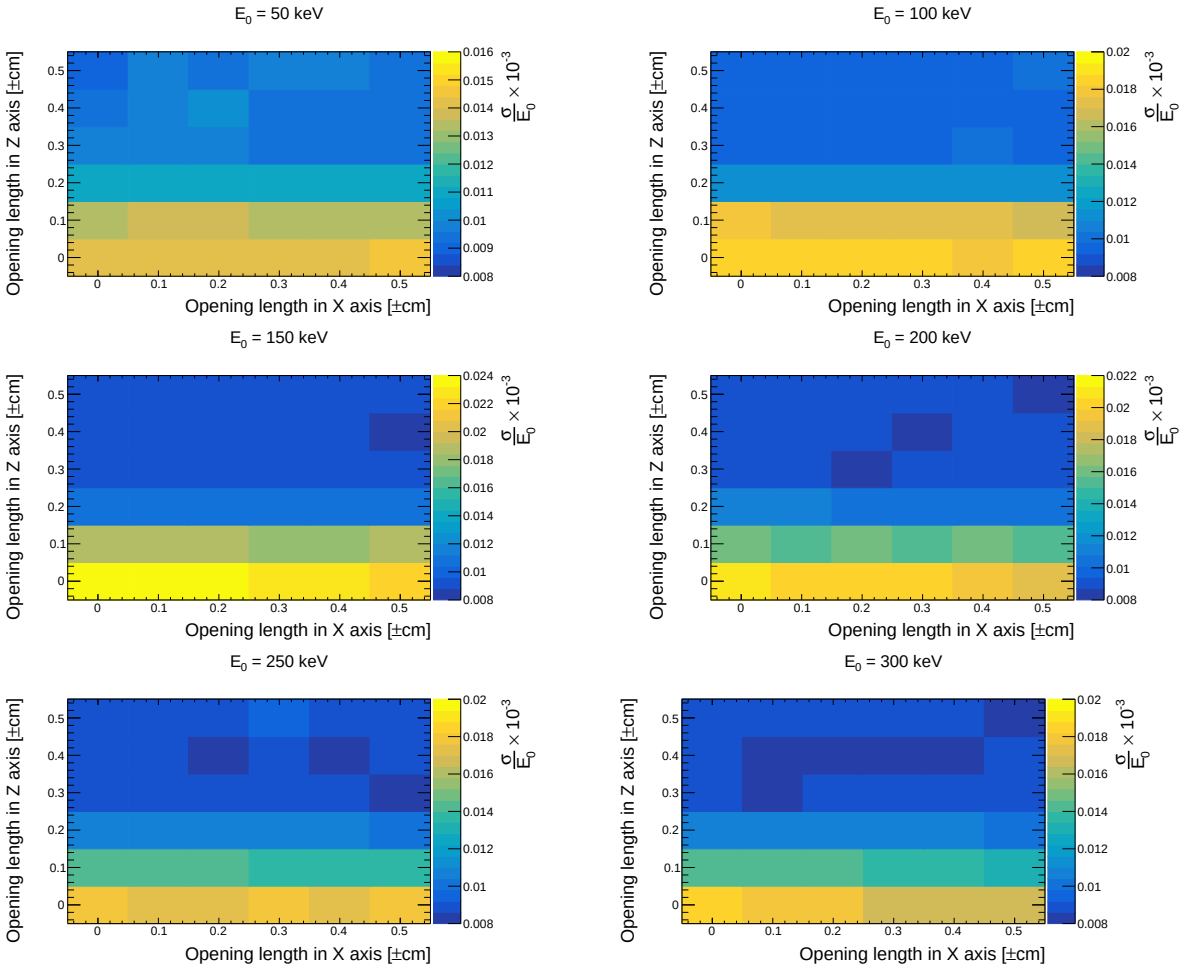

Figure 16: Histograms representing $\frac{\sigma}{E_0} \times 10^{-3}$ in terms of the horizontal and vertical slit opening for primary energies from 50 to 300 keV for small step size

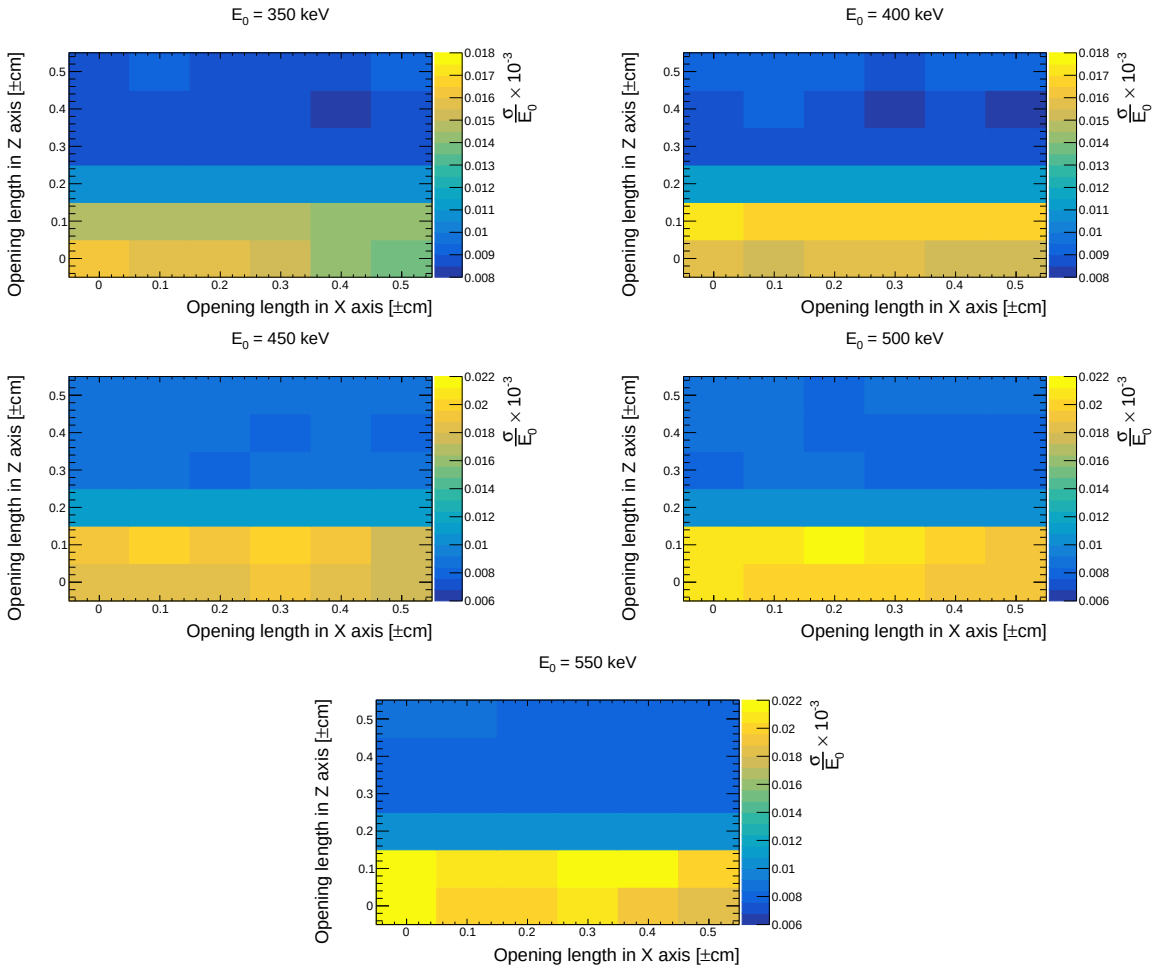

Figure 17: Histograms representing $\frac{\sigma}{E_0} \times 10^{-3}$ in terms of the horizontal and vertical slit opening for primary energies from 350 to 550 keV for small step size

F Reference for the beta spectrometer program

The spectrometer simulation is available in this GitHub page

References

[1] F. Juget. "Etude pour la réalisation d'un spectromètre β à double focalisation". École polytechnique fédérale de Lausanne, 1995.

[2] S. Agostinelli et al. "Geant4—a simulation toolkit". In: *Nucl.Instrum. Methods Phys. Res. A* 506.3 (2003), pp. 250–303.

[3] Alfredo Ferrari et al. "FLUKA: A multi-particle transport code (Program version 2005)". In: (2005).

[4] J. Allison et al. "Geant4 developments and applications". In: *IEEE Trans. Nucl. Sci.* 53.1 (2006), pp. 270–278.

[5] N. D. Gagunashvili. "Comparison of weighted and unweighted histograms". In: *PoS* ACAT (2007), p. 054.

[6] V.O. Sergeev and F.F. Valiev. "Unique second-forbidden β transitions: Decay of 137Cs". In: *Bull. Russ. Acad. Sci. Phys.* 71 (2007), pp. 827–831.

[7] T.T. Böhlen et al. "The FLUKA Code: Developments and Challenges for High Energy and Medical Applications". In: *Nuclear Data Sheets* 120 (2014), pp. 211–214.

[8] F. Juget, C. Bailat, and F. Bochud. "Preliminary beta spectrum measurements using a magnetic spectrometer". In: *Applied Radiation and Isotopes* 87 (2014), pp. 310–314.

[9] X. Mougeot. In: *Physical Review C* 91 (2015), p. 055504.

[10] X. Mougeot. In: *Erratum Phys. Rev. C* 92 (2015), p. 059902.

[11] J. Allison et al. "Recent developments in Geant4". In: *Nucl.Instrum. Methods Phys. Res. A* 835 (2016), pp. 186–225.

[12] M.-M. Bé et al. *Table of Radionuclides*. Vol. 8. Monographie BIPM-5. Sèvres: Bureau International des Poids et Mesures, 2016. ISBN: 978-92-822-2264-5.

[13] J. Nabi et al. "Unique first-forbidden β-decay transitions in odd–odd and even–even heavy nuclei". In: *Nuclear Physics A* 957 (2017), pp. 1–21.

[14] L. Amaral. "Topics on Solid Angles". In: *Journal of Applied Mathematics and Physics* 7 (2019), pp. 2423–2439.

[15] F. Juget et al. "Development and validation of a double focalizing magnetic spectrometer for beta spectrum measurements". In: *Nuclear Inst. and Methods in Physics Research A* 942 (2019), p. 162384.

[16] N. Feliks, M. Jacquart, and M. Berchet. *TP IVa: β-Spectrometer*. École polytechnique fédérale de Lausanne, 2020.

[17] F. Mauger and V. Tretyak. *BxDecay0 - C++ port of the legacy Decay0 FORTRAN library.*

[18] O. Schneider. *Physique Nucléaire et Corpusculaire II*. Leçon 6. Lecture slides. École polytechnique fédérale de Lausanne. 6 March 2021.

[19] F. James. *Statistical methods in experimental physics*. (World Scientific), (2006). ISBN: 978-981-256-795-6, 978-981-270-527-3.